

1 **The effects of orbital precession on tropical precipitation: Mechanisms**
2 **controlling precipitation changes over land and ocean**

3
4
5
6
7
8

9 Kimberly A. Chamales¹, Amy C. Clement¹, Simona Bordoni², and Lisa N. Murphy¹

10
11
12
13
14
15
16
17

18 ¹ Rosenstiel School of Marine and Atmospheric Science, University of Miami, Miami, FL
19 33149, USA

20 ² California Institute of Technology, Pasadena, CA 91125, USA

21

22 Corresponding author address: Kimberly Chamales, RSMAS/MPO 4600 Rickenbacker
23 Causeway, Miami, FL 33149, USA. E-mail: kchamales@rsmas.miami.edu

24 **Key Points**

- 25 1. Models show a land-ocean shift in precipitation due to precessional forcing
- 26 2. Top-of-atmosphere energetic mechanism describes precipitation changes over land
- 27 3. Circulation changes over land drive precipitation changes over ocean

28

29 **Keywords:** Paleoclimate, Precipitation, Precession, Mid-Holocene

30
31
32
33
34
35
36
37
38
39
40
41
42
43
44
45

Abstract

The tropical precipitation response to precessional forcing is investigated using idealized precession experiments from the Geophysical Fluid Dynamics Laboratory Coupled Model version 2.1 and mid-Holocene experiments from ten general circulation models participating in the Paleoclimate Modeling Intercomparison Project Phase III. Both sets of experiments show a seasonal land-ocean asymmetry in the tropical precipitation response: precipitation increases over land and decreases over ocean in the season with increased insolation and the opposite is true in the season with decreased insolation. This response is examined using a framework that describes how changes in net top-of-atmosphere radiation affect the atmosphere and surface energy balances. Over land, surface energy storage is small and changes in precipitation are balanced by changes in moist static energy flux divergence. Over ocean, surface energy storage is large, moist static energy flux divergence is small, and changes in precipitation are ultimately driven by changes in circulation and atmospheric stability.

Index Terms: 3344, 3354

46 **1. Introduction**

47 Earth's orbital variations impact climate over glacial-interglacial timescales by
48 altering the amount of insolation reaching the top of the atmosphere. Orbital precession
49 modulates seasonal insolation and impacts climate on cycles of about 20 kyr.
50 Precessional signals have been observed in a variety of tropical precipitation records
51 including speleothems from Asia and South America [*Cruz et al.*, 2005; *X Wang et al.*,
52 2006; *X Wang et al.*, 2007; *Y Wang et al.*, 2008] and sediment cores from Asia, South
53 America, and Africa [*Street and Grove*, 1979; *F. Gasse et al.*, 1991; *deMenocal et al.*,
54 2000; *Françoise Gasse*, 2000; *Bush et al.*, 2002; *Trauth et al.*, 2003; *Herzschuh*, 2006]
55 Paleorecords also provide evidence that intensified monsoon precipitation occurred
56 during the mid-Holocene, a period about 6 ka that was characterized by enhanced
57 insolation due to precessional forcing [*Winkler and Wang*, 1993; *Yu and Harrison*, 1996;
58 *Jolly et al.*, 1998; *Yu et al.*, 1998; *Kohfeld and Harrison*, 2000; *Baker et al.*, 2001; *Haug*
59 *et al.*, 2001; *Marchant et al.*, 2009]. Understanding the relationship between precessional
60 changes in insolation and precipitation can help explain how precipitation changed in past
61 climates on glacial-interglacial timescales and how it might change in the future.

62 A variety of modeling studies show that a land-ocean shift in precipitation exists
63 as a result of mid-Holocene forcing [*Braconnot et al.*, 2007; *Braconnot et al.*, 2008; *Hsu*
64 *et al.*, 2010; *Bosmans et al.*, 2012; *Zhao and Harrison*, 2012] and idealized precessional
65 forcing [*Tuenter et al.*, 2003; *Clement et al.*, 2004]. Here, the term “idealized” refers to
66 experiments that do not correspond to any specific past climates. This land-ocean shift in
67 precipitation was originally described as land and sea breezes caused by differences in
68 the heating of land and ocean [*Kutzbach and Ottobliesner*, 1982; *COHMAP Members*,

69 1988; *Tuenter et al.*, 2003; *Ruddiman*, 2008; *Bosmans et al.*, 2012]. *Bosmans et al.*
70 [2012] summarize this mechanism and show that increased summer insolation
71 strengthens the thermal low over the warming continents, which increases the land-sea
72 pressure gradient and the monsoon winds. However, *Merlis et al.* [2013a] suggest that
73 changes in precipitation cannot simply be explained through differences in the heating of
74 land and ocean, because changes in the monsoonal circulation are constrained by changes
75 in the atmospheric energy balance rather than by the surface temperature gradient. In an
76 aquaplanet configuration, this can lead to the counterintuitive result of a weaker
77 circulation in the summer with perihelion, despite an increase in the precipitation there
78 [*Merlis et al.*, 2013b]. Hence, *Merlis et al.* [2013a] argue for a more fundamental role of
79 the energetic framework in studies of the tropical precipitation response to radiative
80 perturbations. *Merlis et al.* [2012] develop a framework describing precessional changes
81 in monsoonal circulation in terms of changes in the net top-of-atmosphere (TOA)
82 radiation with idealized aquaplanet simulations, and *Merlis et al.* [2013a] apply the
83 framework to simulations with a zonally symmetric land surface. The purpose of this
84 study is to extend the framework of *Merlis et al.* [2012] and *Merlis et al.* [2013a] to a
85 climate model with a realistic distribution of land and a more complete set of physical
86 processes in order to better understand the tropical hydrological response to precessional
87 forcing.

88 *Hsu et al.* [2010] also discusses the land-ocean asymmetry of tropical
89 precipitation changes in the mid-Holocene using an energetic approach similar to the one
90 used by *Merlis et al.* [2013a]. They use a balance of moist static energy (MSE) and
91 radiative fluxes at the TOA and surface to explain changes in precipitation over land and

92 ocean, and find that the previous season insolation forcing is important for the magnitude
93 of the land-ocean precipitation change; the different heat capacity of land and ocean and
94 the associated slow response time of the ocean allows the insolation forcing of one season
95 to cancel out the insolation forcing of the following season, causing changes in
96 precipitation over ocean to lag the changes in precipitation over land. While this
97 previous-season insolation mechanism accounts for part of the magnitude of the
98 precipitation change, the direct-season insolation is still significant for the presence of the
99 land-ocean contrast. Our study focuses on the mechanism controlling the direct-season
100 response of the precipitation changes. Applying a TOA energetic framework to idealized
101 precession experiments can help elucidate how tropical precipitation changes in response
102 to radiative forcing and highlight the differences in the mechanisms controlling
103 precipitation changes over land and ocean. Using the atmospheric energy budget
104 sidesteps some of the large but canceling terms, such as the convective diabatic heating,
105 that appear in the individual moisture and temperature equations [*Neelin, 2007*]. This
106 approach emphasizes the importance of the net energy input into the atmospheric column
107 and its implications for understanding the precipitation response to changes in the TOA
108 energy.

109 We also examine the changes in tropical precipitation over land and ocean in the
110 Paleoclimate Modeling Intercomparison Project Phase III (PMIP3) mid-Holocene
111 experiments. Analyzing the previously documented land-ocean asymmetry in a suite of
112 climate models with a standardized experimental design can help assess the robustness of
113 this precipitation signal and motivate the need for a complete mechanistic understanding
114 of precessional changes in precipitation.

115 Section 2 describes the models and experiments used in this study. In Section 3,
116 we discuss the seasonal precipitation change over land and ocean in the PMIP3 models,
117 while results from the idealized experiments and mechanisms used to constrain
118 precipitation changes over land and ocean are examined in Section 4. A brief discussion
119 follows in Section 5.

120

121 **2. Methodology**

122 We use two sets of experiments for this study. The first is from PMIP3, a project
123 that aims to coordinate paleoclimate modeling and model evaluation using standardized
124 experiments from various models and research institutions across the globe. Here, we use
125 climatological monthly data from the PMIP3 mid-Holocene and pre-industrial control
126 experiments. Table 1 lists the 10 models used in this study, the model years used to
127 compute each climatology, and the reference for each model.

128 We use mid-Holocene experiments (MH) in which the autumnal equinox is set
129 close to perihelion ($\omega-180=0.87$, where ω is the longitude of perihelion), and
130 preindustrial control experiments (PI) in which the Northern Hemisphere (NH) winter
131 solstice occurs near perihelion ($\omega-180=102.04$). Further details of the forcings and
132 boundary conditions can be found on the PMIP3 website (<https://pmip3.lsce.ipsl.fr/>).
133 Although there are slight variations in the greenhouse gas concentrations prescribed for
134 MH and PI, the changes resulting from those forcings are small compared to those
135 resulting from the orbital forcing [*Bosmans et al.*, 2012]. We examine the multi-model
136 mean of the difference in the monthly climatologies between the two experiments (MH-
137 PI).

138 To examine in more detail the mechanisms controlling the precession-induced
139 shift in precipitation between land and ocean, we use idealized simulations from the
140 Geophysical Fluid Dynamics Laboratory (GFDL) Coupled Model version 2.1 (CM2.1).
141 The atmosphere and land components have a horizontal resolution of 2° latitude x 2.5°
142 longitude, and the atmosphere has 24 vertical levels. The ocean model has a horizontal
143 resolution of 1° latitude x 1° longitude – with a latitudinal resolution that gradually
144 decreases equatorward of 30° so that it is 1/3° at the equator – and 50 vertical levels
145 [*Delworth et al.*, 2006].

146 We use two experiments in which the precessional signal is stronger than in the
147 mid-Holocene experiments. In the first experiment (hereafter referred to as the summer
148 solstice experiment "SS"), perihelion is set at the NH summer solstice ($\omega-180=270$) and
149 in the second experiment (hereafter referred to as the winter solstice experiment "WS"),
150 perihelion is set at the NH winter solstice ($\omega-180=90$). Because eccentricity modulates
151 the strength of precessional forcing [*Jackson and Broccoli*, 2003], eccentricity is
152 increased to 0.0493 in order to maximize the model's response to the precessional
153 forcing. All other parameters are set to pre-industrial levels. A complete description of
154 the experimental design can be found in *Erb et al.* [2013]. The simulations were run for
155 600 years of which we examine the last 100 years and compute the monthly mean climate
156 changes between the two experiments (SS-WS).

157

158 **3. Precipitation Changes During the Mid-Holocene**

159 It is of interest to first determine if today's climate models show a robust
160 precipitation signal over land and ocean in response to changes in orbital precession. We

161 do this by examining the multi-model mean seasonal cycle of precipitation change over
 162 tropical land and ocean in the PMIP3 models (Fig. 1). In boreal summer, the precipitation
 163 change is positive over land and negative over ocean, indicating that the season with
 164 enhanced insolation also receives enhanced precipitation over land. The opposite is true
 165 in boreal winter: the earth receives less insolation, and the change in precipitation is
 166 negative over land and positive over ocean. This result shows that ten of the climate
 167 models that participated in PMIP3 respond with a robust land-ocean shift in precipitation,
 168 reinforcing the importance of understanding the mechanisms that drive this distinct
 169 precipitation signal.

170

171 **4. Precipitation Changes in Idealized Experiments**

172 **4.1. TOA Energetic Mechanism**

173 We now adopt the energetic framework used by *Merlis et al.* [2013a] who
 174 constrained the response of the monsoonal Hadley circulation to precessional forcing
 175 with an energy budget at the TOA. Their framework was applied to idealized model
 176 simulations with a zonally symmetric continent. Here, we extend this framework to
 177 GFDL-CM2.1, which has a realistic land configuration.

178 From *Merlis et al.* [2013a], the energy balance of the atmosphere and surface is

$$179 \quad \left\{ \frac{\partial \bar{E}}{\partial t} \right\} + \rho_o c_{po} d \frac{\partial \bar{T}_s}{\partial t} = S_{TOA} - L_{TOA} - \nabla \cdot \{ \overline{\mathbf{v}h} \} - \nabla \cdot \mathbf{F}_o, \quad (1)$$

180

181 where the time-mean is denoted by $\overline{(\cdot)}$ and the vertically mass-weighted integral is
 182 denoted by $\{\cdot\}$. $E = c_v T + gz + Lq$ is the total atmospheric energy and $h = c_p T + gz +$
 183 Lq is the MSE. S_{TOA} is the net TOA shortwave radiation, L_{TOA} is the net TOA longwave

184 radiation, ρ_o is the ocean density, c_{po} is the ocean heat capacity, d is the mixed layer
 185 depth, T_s is the surface temperature, $\nabla \cdot F_o$ is the ocean energy flux divergence, and
 186 $\nabla \cdot \{\overline{\mathbf{v}h}\}$ is the atmospheric MSE flux divergence, where \mathbf{v} is the horizontal winds. If
 187 atmospheric and land energy storage are considered negligible, the balance in (1)
 188 becomes

$$189 \quad S_{TOA} - L_{TOA} \approx A\rho_o c_{po} d \frac{\delta \overline{T_s}}{\delta t} + \nabla \cdot \{\overline{\mathbf{v}h}\} + \nabla \cdot F_o, \quad (2)$$

190 where

$$A = \begin{cases} 1 & \text{over ocean} \\ 0 & \text{over land.} \end{cases}$$

191

192 If we consider insolation changes, the perturbation energy balance becomes

$$193 \quad \delta(S_{TOA} - L_{TOA}) \approx A\rho_o c_{po} d \delta \frac{\delta \overline{T_s}}{\delta t} + \delta \nabla \cdot \{\overline{\mathbf{v}h}\} + \delta \nabla \cdot F_o. \quad (3)$$

194

195 Over land, the surface storage term and the ocean energy flux divergence are
 196 zero, so changes in the net (shortwave minus longwave) TOA radiation are balanced
 197 solely by changes in MSE flux divergence. Over ocean, changes in net TOA radiation can
 198 be balanced by changes in MSE flux divergence, ocean energy flux divergence, and
 199 surface energy storage.

200 While Eq. (3) is useful because it describes the energy balance of the atmosphere
 201 and the surface, it does not explicitly account for changes in precipitation. In order to
 202 understand how changes in net TOA radiation lead to changes in precipitation, we link
 203 the energy and moisture budgets by considering the atmosphere in equilibrium. The
 204 surface warms through radiative heating and convection heats the upper atmosphere

205 through precipitation and latent heat release. Therefore, in monsoon regions where
206 sufficient surface moisture is available, changes in net TOA radiation over land are
207 balanced by changes in precipitation:

$$208 \quad \delta P_L \approx \delta(S_{TOA} - L_{TOA}) \approx \delta \nabla \cdot \{\overline{vh}\}, \quad (4)$$

209

210 where P_L is the precipitation over land.

211

212 **4.2. Results**

213 Similar to the mid-Holocene experiments, a land-ocean asymmetry in
214 precipitation exists as a result of the idealized precessional forcing in the GFDL-CM2.1
215 simulations (Fig. 2). In order to examine the mechanism driving this precipitation signal,
216 we examine the tropical-mean changes in net TOA radiation, net surface fluxes, and MSE
217 flux divergence over land and ocean for both models. As expected from Eqs. (3) and (4),
218 changes in precipitation have the same sign as the changes in net TOA radiation over
219 land surfaces. Energy is redistributed from the surface to the atmosphere through vertical
220 motion, which results in convection and latent heat release. Therefore, over land,
221 increases in net TOA radiation correspond to increases in precipitation and decreases in
222 net TOA radiation correspond to decreases in precipitation.

223 Over ocean, the sign of the change in net TOA radiative forcing is the same as it
224 is over land, but the change in precipitation is opposite. This difference arises as a result
225 of the ocean energy storage: Fig. 2 indicates that over ocean, changes in net TOA
226 radiation are almost entirely balanced by changes in the surface energy fluxes. The
227 surface storage term dominates over the ocean heat flux divergence term (not shown)

228 indicating that the energy flux is warming or cooling the ocean surface. The ocean
229 responds to the increase in net TOA radiation during boreal summer by absorbing energy
230 and warming the surface, and it responds to the decrease in net TOA radiation during
231 boreal winter by releasing energy and cooling the surface. As a result, the change in MSE
232 flux divergence over ocean is very small; the atmosphere over ocean does much less
233 work to adjust to the TOA forcing than the atmosphere over land.

234 While this analysis is useful for understanding the atmospheric energy budget
235 over both land and ocean, it does not explicitly explain why precipitation decreases over
236 ocean when net TOA radiation is increasing, and vice versa. To further understand the
237 oceanic precipitation response, we examine the seasonal cycle of the moisture flux
238 divergence over ocean.

239 As in *Clement et al.* [2004], we decompose the moisture flux convergence into the
240 effects of the circulation changes, $-\nabla \cdot \{\mathbf{v}'\bar{q}\}$, and the effects of the moisture changes,
241 $-\nabla \cdot \{\bar{\mathbf{v}}q'\}$, where q is the specific humidity, $\overline{(\cdot)}$ denotes the mean (WS) field and $(\cdot)'$
242 denotes a deviation from the mean. Fig. 3 shows the change in the seasonal cycle of these
243 terms over ocean. It is evident that the seasonal change in circulation, i.e., the dynamic
244 component, dominates the seasonal change in the specific humidity, i.e., the
245 thermodynamic component (this also true over land, not shown). The effect of the
246 circulation change is such that moisture is diverging over ocean in boreal summer and
247 converging over ocean in boreal winter. This is consistent with the change in
248 precipitation over ocean. We deduce from Fig. 3 that a dynamic mechanism is controlling
249 precipitation changes over ocean (i.e., subsidence and decreased precipitation during
250 boreal summer and ascent and increased precipitation during boreal winter). This differs

251 from the mechanism controlling precipitation changes over land, which is dictated by the
252 atmospheric energy response to a change in net TOA radiation.

253 The thermodynamic structure of the atmosphere may be necessary to explain how
254 precipitation can change over ocean despite little change in the MSE flux divergence.
255 Fig. 4 shows the change in the vertical profiles of the dry and latent energy over land and
256 ocean in boreal winter (DJF) and boreal summer (JJA). The dry energy is taken as $c_p\theta$,
257 where θ is the potential temperature and c_p is the specific heat for dry air, and latent
258 energy is taken as L_vq , where L_v is the latent heat of vaporization. The latent energy is
259 most important in the lower levels of the troposphere, and it decreases during DJF when
260 the surface is cooling and increases in JJA when the surface is warming. The profile of
261 $c_p\theta$ has small seasonal change over land and a larger change over ocean. Here, the
262 atmosphere becomes more unstable ($d\theta/dp > 0$) in DJF and more stable ($d\theta/dp < 0$) in
263 JJA.

264 We suggest that a reorganization of the thermodynamic structure of the
265 atmosphere over ocean, which is driven by circulation changes over land, may ultimately
266 allow for a change in precipitation. For example, in boreal summer when there is a net
267 gain in the TOA radiation, the atmosphere over land responds to this forcing through an
268 export of MSE, which is achieved through anomalous vertical motion and an increase in
269 precipitation. It is this circulation change over land that drives anomalous descent over
270 ocean. As we saw in the previous section, the atmosphere over ocean does not import
271 more energy; it may instead adjust by becoming more stable, consistent with less rainfall
272 over ocean.
273

274 **5. Discussion**

275 We examined the precipitation response to mid-Holocene and idealized
276 precessional forcing using a variety of climate models. All models agree that a land-
277 ocean shift in precipitation exists as a result of precessional forcing. The idealized
278 simulations were used to examine the mechanisms controlling this distinct precipitation
279 response. We found that while the TOA energetic mechanism outlined in *Merlis et al.*
280 [2013a] explains how precipitation over land responds to precessional forcing, it does not
281 fully explain the precipitation response over ocean.

282 The fundamental constraint dictating the energy balance and resulting
283 precipitation change over land and ocean lies in the surface boundary condition. Over
284 land, the surface stores very little energy and the atmosphere is required to do all the
285 work to compensate for the net TOA energy imbalance. We see this in the MSE flux
286 divergence: as the net TOA radiation increases, the atmosphere responds by diverging
287 MSE and latent heat is released through an increase in precipitation, and as net TOA
288 radiation decreases, the atmosphere converges MSE to maintain equilibrium and
289 precipitation decreases. Over ocean, the energy balance is not so simple because surface
290 energy storage plays an important role in balancing the TOA energy fluxes. When the net
291 TOA radiation increases over ocean, the surface warms and the change in MSE flux
292 divergence does not need to be as large as it is over land. When there is a decrease in the
293 net TOA radiation, the ocean surface cools and, again, the change in MSE flux
294 divergence over ocean is small. Therefore, it is the differing surface properties of the land
295 and ocean that allow for very different atmospheric responses to precessional forcing.

296 While these changes in the energy budgets of the atmosphere and surface are
297 useful for understanding the precipitation response to precessional forcing over land, they
298 do not explicitly explain the land-ocean asymmetry. Analyses of the change in moisture
299 flux convergence and the dry and latent vertical energy profiles of the atmosphere
300 suggest that the atmospheric energy response over land may drive changes in circulation
301 that affect the thermodynamic structure over ocean, allowing for changes in precipitation
302 to occur.

303 Further insight into this mechanism for describing precipitation changes may
304 provide more details of the climate response to precession than mechanisms traditionally
305 invoked in monsoon dynamics. Understanding the mechanisms that drive changes in
306 precipitation due to precessional forcing can not only help explain precipitation changes
307 in past and future climates, but it can also help explain how the precipitation signal
308 manifests in regional climate records. Moreover, it is of interest to examine regional
309 precipitation changes because over glacial-interglacial timescales, the regional response
310 to solar forcing may differ significantly from the global response [*Clement et al.*, 2004].
311 This has important implications for the interpretation of climate records and for regional
312 climate sensitivity.

313

Acknowledgements

314 We would like to thank Michael Erb and Tony Broccoli for providing the data for the
315 GFDL-CM2.1 idealized simulations. Data is available from K.A.C. upon request and
316 additionally, the PMIP3 data can be found online at <http://pcmdi9.llnl.gov/esgf-web-fe/>.
317 This study was supported by the National Science Foundation Paleo Perspectives on
318 Climate Change program.

References

- 319
- 320 Baker, P. A., G. O. Seltzer, S. C. Fritz, R. B. Dunbar, M. J. Grove, P. M. Tapia, S. L.
321 Cross, H. D. Rowe, and J. P. Broda (2001), The history of South American
322 tropical precipitation for the past 25,000 years, *Science*, 291(5504), 640-643,
323 doi:10.1126/science.291.5504.640.
- 324 Bao, Q., et al. (2013), The Flexible Global Ocean-Atmosphere-Land system model,
325 Spectral Version 2: FGOALS-s2, *Advances in Atmospheric Sciences*, 30(3), 561-
326 576, doi:10.1007/s00376-012-2113-9.
- 327 Bosmans, J. H. C., S. S. Drijfhout, E. Tuenter, L. J. Lourens, F. J. Hilgen, and S. L.
328 Weber (2012), Monsoonal response to mid-holocene orbital forcing in a high
329 resolution GCM, *Climate of the Past*, 8(2), 723-740, doi:10.5194/cp-8-723-2012.
- 330 Braconnot, P., C. Marzin, L. Grégoire, E. Mosquet, and O. Marti (2008), Monsoon
331 response to changes in Earth's orbital parameters: comparisons between
332 simulations of the Eemian and of the Holocene, *Climate of the Past*, 4, 281-294.
- 333 Braconnot, P., et al. (2007), Results of PMIP2 coupled simulations of the Mid-Holocene
334 and Last Glacial Maximum - Part 1: experiments and large-scale features, *Climate*
335 *of the Past*, 3(2), 261-277.
- 336 Bush, M. B., M. C. Miller, P. E. De Oliveira, and P. A. Colinvaux (2002), Orbital forcing
337 signal in sediments of two Amazonian lakes, *Journal of Paleolimnology*, 27, 341-
338 352.
- 339 Clement, A. C., A. Hall, and A. J. Broccoli (2004), The importance of precessional
340 signals in the tropical climate, *Climate Dynamics*, 22(4), 327-341,
341 doi:10.1007/s00382-003-0375-8.

342 COHMAP Members (1988), Climatic changes of the last 18,000 years: Observations and
343 model simulations, *Science*, 241(4869), 1043-1052,
344 doi:10.1126/science.241.4869.1043.

345 Cruz, F. W., S. J. Burns, I. Karmann, W. D. Sharp, M. Vuille, A. O. Cardoso, J. A.
346 Ferrari, P. L. S. Dias, and O. Viana (2005), Insolation-driven changes in
347 atmospheric circulation over the past 116,000 years in subtropical Brazil, *Nature*,
348 434(7029), 63-66, doi:10.1038/nature03365.

349 Delworth, T. L., et al. (2006), GFDL's CM2 global coupled climate models. Part I:
350 Formulation and simulation characteristics, *Journal of Climate*, 19(5), 643-674,
351 doi:10.1175/jcli3629.1.

352 deMenocal, P., J. Ortiz, T. Guilderson, J. Adkins, M. Sarnthein, L. Baker, and M.
353 Yarusinsky (2000), Abrupt onset and termination of the African Humid Period:
354 rapid climate responses to gradual insolation forcing, *Quaternary Science*
355 *Reviews*, 19(1-5), 347-361, doi:10.1016/s0277-3791(99)00081-5.

356 Dufresne, J. L., et al. (2013), Climate change projections using the IPSL-CM5 Earth
357 System Model: from CMIP3 to CMIP5, *Climate Dynamics*, 40(9-10), 2123-2165,
358 doi:10.1007/s00382-012-1636-1.

359 Erb, M. P., A. J. Broccoli, and A. C. Clement (2013), The contribution of radiative
360 feedbacks to orbitally driven climate change, *Journal of Climate*, 26(16), 5897-
361 5914, doi:10.1175/jcli-d-12-00419.1.

362 Gasse, F. (2000), Hydrological changes in the African tropics since the Last Glacial
363 Maximum, *Quaternary Science Reviews*, 19(1-5), 189-211, doi:10.1016/S0277-
364 3791(99)00061-X.

365 Gasse, F., et al. (1991), A 13,000-year climate record from Western Tibet, *Nature*,
366 353(6346), 742-745, doi:10.1038/353742a0.

367 Gent, P. R., et al. (2011), The Community Climate System Model Version 4, *Journal of*
368 *Climate*, 24(19), 4973-4991, doi:10.1175/2011jcli4083.1.

369 Giorgetta, M. A., et al. (2013), Climate and carbon cycle changes from 1850 to 2100 in
370 MPI-ESM simulations for the Coupled Model Intercomparison Project phase 5,
371 *Journal of Advances in Modeling Earth Systems*, 5(3), 572-597,
372 doi:10.1002/jame.20038.

373 Haug, G. H., K. A. Hughen, D. M. Sigman, L. C. Peterson, and U. Rohl (2001),
374 Southward migration of the intertropical convergence zone through the Holocene,
375 *Science*, 293(5533), 1304-1308, doi:10.1126/science.1059725.

376 Herzschuh, U. (2006), Palaeo-moisture evolution in monsoonal Central Asia during the
377 last 50,000 years, *Quaternary Science Reviews*, 25(1-2), 163-178,
378 doi:10.1016/j.quascirev.2005.02.006.

379 Hsu, Y.-H., C. Chou, and K.-Y. Wei (2010), Land–ocean asymmetry of tropical
380 precipitation changes in the Mid-Holocene, *Journal of Climate*, 23(15), 4133-
381 4151, doi:10.1175/2010jcli3392.1.

382 Jackson, C. S., and A. J. Broccoli (2003), Orbital forcing of Arctic climate: mechanisms
383 of climate response and implications for continental glaciation, *Climate*
384 *Dynamics*, 21(7-8), 539-557, doi:10.1007/s00382-003-0351-3.

385 Jolly, D., et al. (1998), Biome reconstruction from pollen and plant macrofossil data for
386 Africa and the Arabian peninsula at 0 and 6000 years, *Journal of Biogeography*,
387 25(6), 1007-1027, doi:10.1046/j.1365-2699.1998.00238.x.

388 Kohfeld, K. E., and S. P. Harrison (2000), How well can we simulate past climates?
389 Evaluating the models using global palaeoenvironmental datasets, *Quaternary*
390 *Science Reviews*, 19(1-5), 321-346, doi:10.1016/s0277-3791(99)00068-2.

391 Kutzbach, J. E., and B. L. Ottobliesner (1982), The sensitivity of the African-Asian
392 monsoonal climate to orbital parameter changes for 9,000 years BP in a low-
393 resolution general-circulation model, *Journal of the Atmospheric Sciences*, 39(6),
394 1177-1188, doi:10.1175/1520-0469(1982)039<1177:tsotaa>2.0.co;2.

395 Li, L. J., et al. (2013), The flexible global ocean-atmosphere-land system model, Grid-
396 point Version 2: FGOALS-g2, *Advances in Atmospheric Sciences*, 30(3), 543-
397 560, doi:10.1007/s00376-012-2140-6.

398 Marchant, R., et al. (2009), Pollen-based biome reconstructions for Latin America at 0,
399 6000 and 18 000 radiocarbon years ago, *Climate of the Past*, 5(4), 725-767.

400 Merlis, T. M., T. Schneider, S. Bordoni, and I. Eisenman (2012), Hadley circulation
401 response to orbital precession. Part I: Aquaplanets, *Journal of Climate*, 26(3),
402 740-753, doi:10.1175/JCLI-D-11-00716.1.

403 Merlis, T. M., T. Schneider, S. Bordoni, and I. Eisenman (2013a), Hadley circulation
404 response to orbital precession. Part II: Subtropical continent, *Journal of Climate*,
405 26(3), 754-771, doi:10.1175/jcli-d-12-00149.1.

406 Merlis, T. M., T. Schneider, S. Bordoni, and I. Eisenman (2013b), The tropical
407 precipitation response to orbital precession, *Journal of Climate*, 26(6), 2010-2021,
408 doi:10.1175/jcli-d-12-00186.1.

409 Neelin, J. D. (2007), Moist dynamics of tropical convection zones in monsoons,
410 teleconnections and global warming, in *The Global Circulation of the*

411 *Atmosphere*, edited by T. Schneider and A. Sobel, p. 385, Princeton University
412 Press, Princeton.

413 Phipps, S. J., L. D. Rotstayn, H. B. Gordon, J. L. Roberts, A. C. Hirst, and W. F. Budd
414 (2011), The CSIRO Mk3L climate system model version 1.0-Part 1: Description
415 and evaluation, *Geoscientific Model Development*, 4(2), 483-509,
416 doi:10.5194/gmd-4-483-2011.

417 Ruddiman, W. F. (2008), *Earth's Climate: Past and Future*, 2nd ed., W. H. Freeman &
418 Company.

419 Schmidt, G. A., et al. (2014), Configuration and assessment of the GISS ModelE2
420 contributions to the CMIP5 archive, *Journal of Advances in Modeling Earth
421 Systems*, 6(1), 141-184, doi:10.1002/2013ms000265.

422 Street, F. A., and A. T. Grove (1979), Global maps of lake-level fluctuations since 30,000
423 yr BP, *Quaternary Research*, 12(1), 83-118, doi:10.1016/0033-5894(79)90092-9.

424 Trauth, M. H., A. L. Deino, A. G. N. Bergner, and M. R. Strecker (2003), East African
425 climate change and orbital forcing during the last 175 kyr BP, *Earth and
426 Planetary Science Letters*, 206(3-4), 297-313, doi:10.1016/s0012-821x(02)01105-
427 6.

428 Tüenter, E., S. L. Weber, F. J. Hilgen, and L. J. Lourens (2003), The response of the
429 African summer monsoon to remote and local forcing due to precession and
430 obliquity, *Global and Planetary Change*, 36(4), 219-235, doi:10.1016/s0921-
431 8181(02)00196-0.

432 Voltaire, A., et al. (2013), The CNRM-CM5.1 global climate model: description and
433 basic evaluation, *Climate Dynamics*, 40(9-10), 2091-2121, doi:10.1007/s00382-
434 011-1259-y.

435 Wang, X., A. S. Auler, R. L. Edwards, H. Cheng, E. Ito, and M. Solheid (2006),
436 Interhemispheric anti-phasing of rainfall during the last glacial period,
437 *Quaternary Science Reviews*, 25(23-24), 3391-3403,
438 doi:10.1016/j.quascirev.2006.02.009.

439 Wang, X., A. S. Auler, R. L. Edwards, H. Cheng, E. Ito, Y. Wang, X. Kong, and M.
440 Solheid (2007), Millennial-scale precipitation changes in southern Brazil over the
441 past 90,000 years, *Geophysical Research Letters*, 34(23),
442 doi:10.1029/2007gl031149.

443 Wang, Y., H. Cheng, R. L. Edwards, X. Kong, X. Shao, S. Chen, J. Wu, X. Jiang, X.
444 Wang, and Z. An (2008), Millennial- and orbital-scale changes in the East Asian
445 monsoon over the past 224,000 years, *Nature*, 451(7182), 1090-1093,
446 doi:10.1038/nature06692.

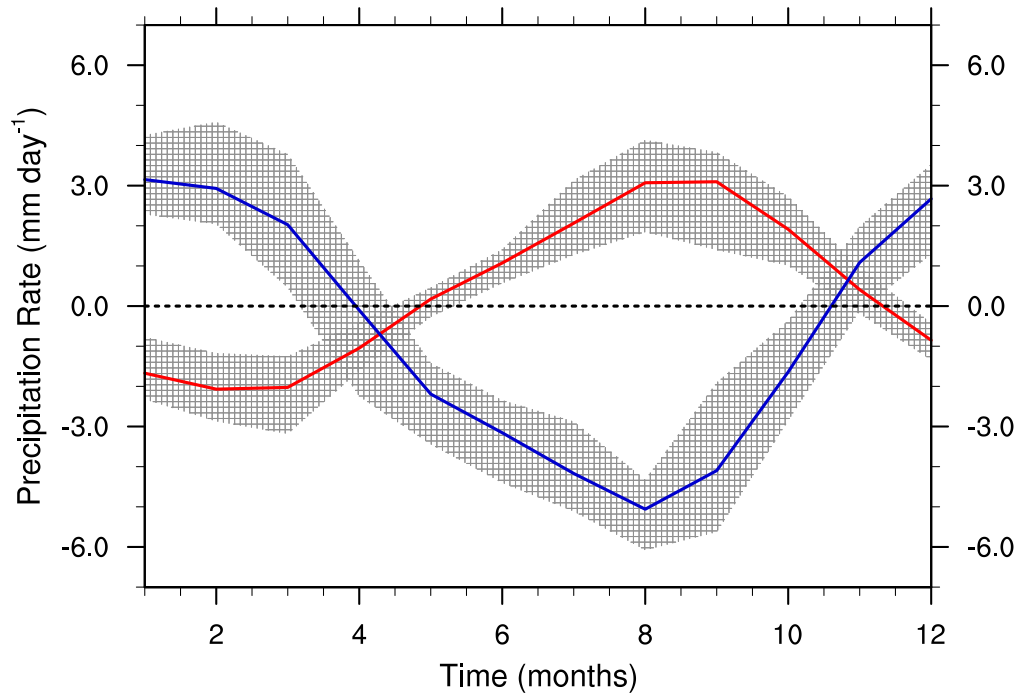
447 Watanabe, S., et al. (2011), MIROC-ESM 2010: Model description and basic results of
448 CMIP5-20c3m experiments, *Geoscientific Model Development*, 4(4), 845-872,
449 doi:10.5194/gmd-4-845-2011.

450 Winkler, M. G., and P. K. Wang (1993), The Late-Quaternary Vegetation and Climate of
451 China, in *Global Climates Since the Last Glacial Maximum*, edited by H. E.
452 Wright, J. E. Kutzbach, T. Webb III, W. F. Ruddiman, F. A. Street-Perrott and P.
453 J. Bartlein, pp. 221-261, University of Minnesota Press, Minneapolis.

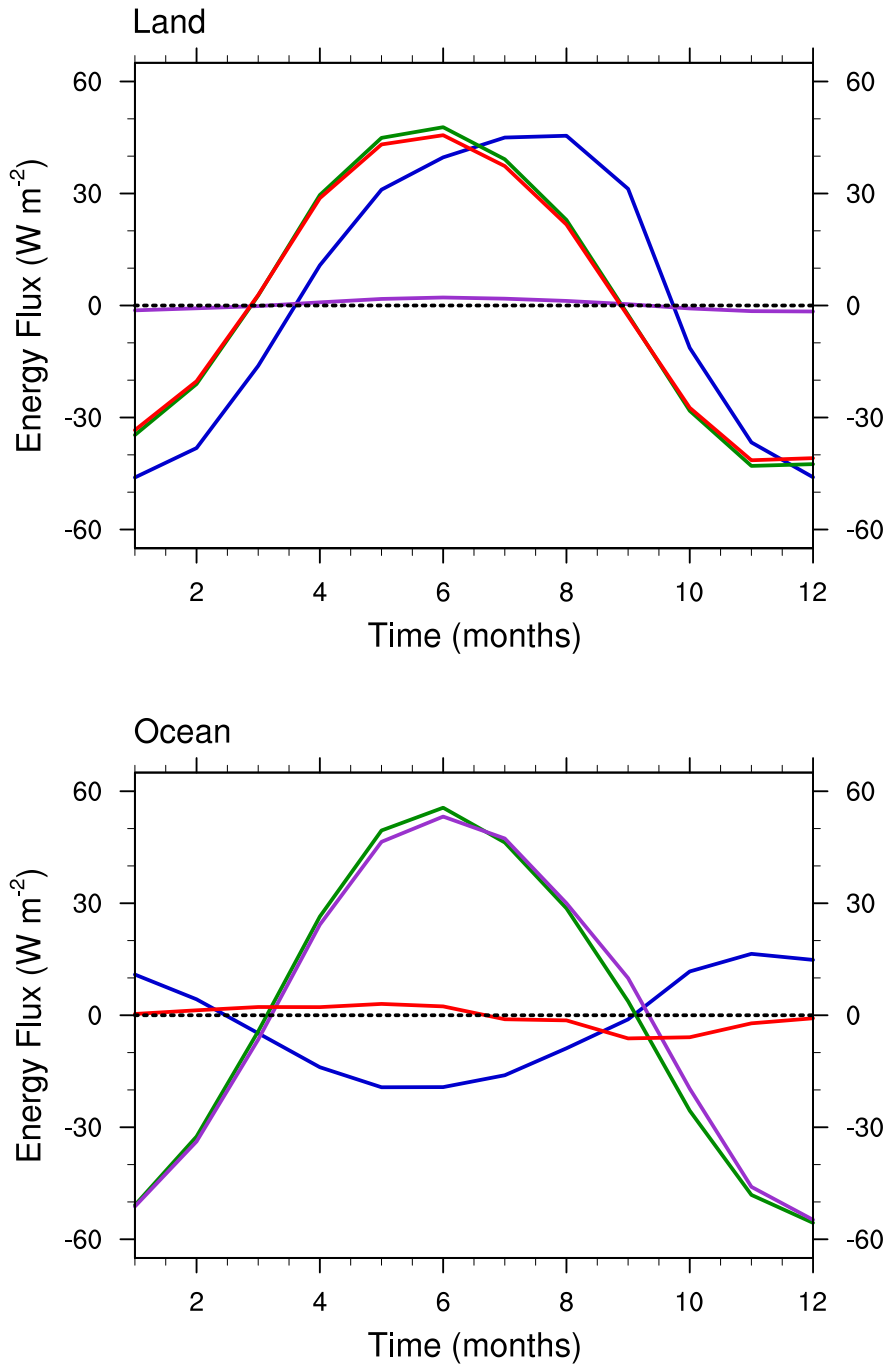
- 454 Yu, G., and S. P. Harrison (1996), An evaluation of the simulated water balance of
455 Eurasia and northern Africa at 6000 y BP using lake status data, *Climate*
456 *Dynamics*, 12(11), 723-735, doi:10.1007/s003820050139.
- 457 Yu, G., I. C. Prentice, S. P. Harrison, and X. J. Sun (1998), Pollen-based biome
458 reconstructions for China at 0 and 6000 years, *Journal of Biogeography*, 25(6),
459 1055-1069, doi:10.1046/j.1365-2699.1998.00237.x.
- 460 Yukimoto, S., et al. (2012), A new global climate model of the Meteorological Research
461 Institute: MRI-CGCM3-Model description and basic performance, *Journal of the*
462 *Meteorological Society of Japan*, 90A, 23-64, doi:10.2151/jmsj.2012-A02.
- 463 Zhao, Y., and S. P. Harrison (2012), Mid-Holocene monsoons: a multi-model analysis of
464 the inter-hemispheric differences in the responses to orbital forcing and ocean
465 feedbacks, *Climate Dynamics*, 39, 1457–1487, doi:10.1007/s00382-011-1193-z.

Model Name	Model Years for Climatology		Reference
	MH	PI	
CCSM4	1000-1300	250-1300	<i>Gent et al.</i> [2011]
CNRM-CM5	1950-2149	1850-2699	<i>Voldoire et al.</i> [2013]
CSIRO-Mk3L-1-2	1-500	1-1000	<i>Phipps et al.</i> [2011]
FGOALS-g2	340-1024	201-900	<i>Li et al.</i> [2013]
FGOALS-s2	1-100	1850-2350	<i>Bao et al.</i> [2013]
GISS-E2-R	2500-2599	3331-4530	<i>Schmidt et al.</i> [2014]
IPSL-CM5A-LR	2301-2800	1800-2799	<i>Dufresne et al.</i> [2013]
MIROC-ESM	2330-2429	1800-2429	<i>Watanabe et al.</i> [2011]
MPI-ESM-P	1850-1949	1850-3005	<i>Giorgetta et al.</i> [2013]
MRI-CGCM3	1951-2050	1851-2350	<i>Yukimoto et al.</i> [2012]

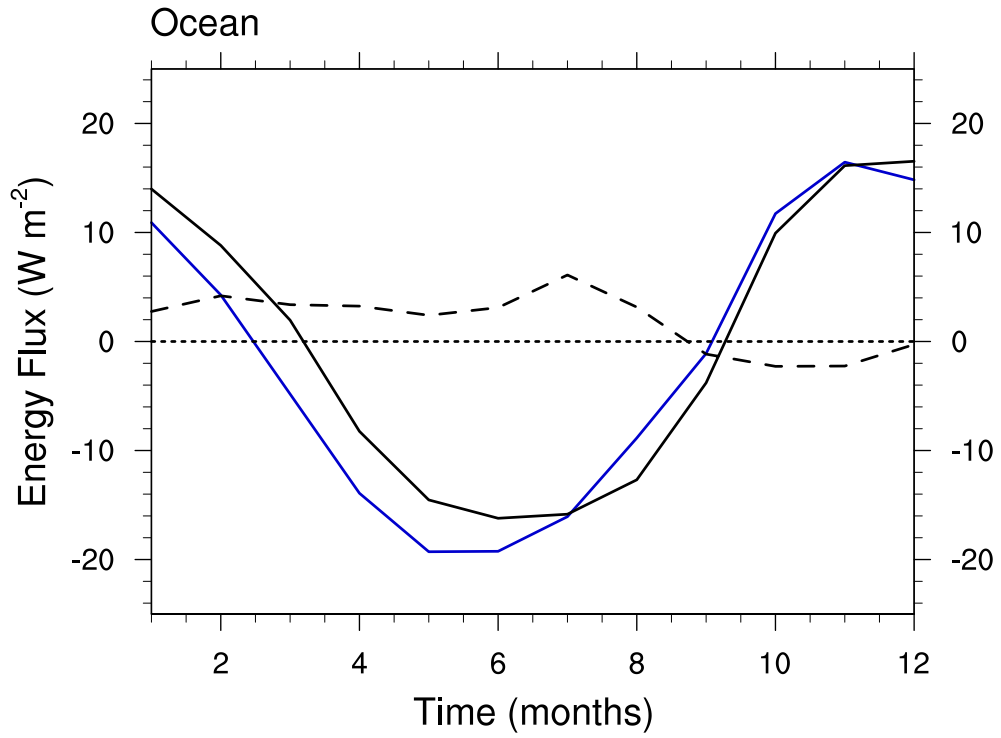
466 Table 1. PMIP3 models used in this analysis, model years averaged over for the mid-
467 Holocene and pre-industrial climatologies, and references.



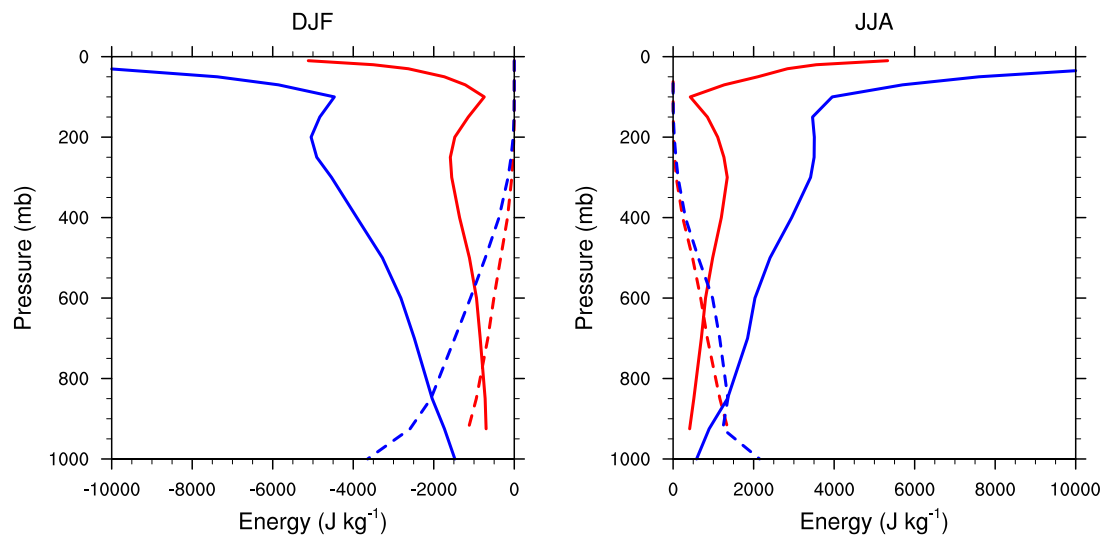
468 Figure 1: Multi-model mean seasonal cycle of the precipitation difference as a function of
 469 time between experiments (MH-PI) for the 10 PMIP3 models (listed in Table 1) over land
 470 (red) and ocean (blue). Shading indicates the model spread. Curves are scaled by the
 471 percentage of land and ocean in the tropics.



472 Figure 2: Seasonal cycle of the difference (SS-WS) in tropical-mean (30°N to 30°S)
 473 precipitation (blue), net TOA radiation (green), net surface energy fluxes (purple), and
 474 MSE flux divergence (red) as a function of time over land and ocean for GFDL-CM2.1.



475 Figure 3: Seasonal cycle of the difference (SS-WS) in tropical-mean (30°N to 30°S)
 476 precipitation (blue) and moisture flux convergence broken down into circulation changes
 477 (solid) and specific humidity changes (dashed) as a function of time over ocean for
 478 GFDL-CM2.1.



479 Figure 4: Vertical profile of the difference (SS-WS) in tropical-mean (30°N to 30°S) dry
 480 (solid) and latent (dashed) energy as a function of pressure over land (red) and ocean
 481 (blue) for GFDL-CM2.1. Curves are scaled by the percentage of land and ocean in the
 482 tropics.